Macromolecular Materials and Engineering
www.mme-journal.de

Polymer Crystallization Studied by Hyphenated Rheology Techniques: Rheo-NMR, Rheo-SAXS, and Rheo-Microscopy

*Volker Räntzsch, Mürüvvet Begüm Özen, Karl-Friedrich Ratzsch, Eric Stellamanns, Michael Sprung, Gisela Guthausen, and Manfred Wilhelm**

Rheological set-ups with in situ analytical sensors, combine information on the flow and deformation behavior of soft matter, with simultaneous insights into structural and dynamic features. Furthermore, they permit the study of soft matter under well-defined flow conditions. Herein are presented hyphenations of rheology and nuclear magnetic resonance (NMR), small angle X-ray scattering (SAXS), and optical microscopy. They are employed to unravel relationships between the molecular dynamics, morphology, and rheology of crystallizing polymers. The results confirm a physical gelation process during polymer crystallization, mediated by the interaction of growing superstructures at volume fractions of 10–15%. The buildup of row-nucleated structures during flow-induced crystallization is found to reduce the time of gelation as detected by the rheological response. These investigations help to clarify the crystallization mechanism, structure–property relationships, and the hardening behavior of crystallizing polymers.

1. Introduction

The interest in understanding every detail of polymer crystallization continues to be intense because of its mechanistic complexity, the variety of structure–property relationships, and the enormous commercial relevance of synthetic semi-crystalline polymers.[1–4] Achieving control over the hierarchical structure of semi-crystalline polymers on the nano-, meso-, and macroscale is a crucial aspect in the targeted design of material properties. The semi-crystalline morphology of polymers depends highly on the molecular-weight distribution, chain topology, stereo- and regio-regularity, additives, and crystallization conditions.[5–10] In injection molding, film blowing, or fiber spinning, polymer melts are crystallized under strong flows which has a strong impact on the resulting micro-structure of the materials (**Figure 1**).[11–15] Applied temperature, pressure, flow rates and their durations, and absolute deformations are critical parameters in achieving increased nucleation and row-nucleated morphologies.[16–18]

In order to use semi-crystalline polymers in new processes such as 3D printing, micro-molding, or electrospinning, a precise knowledge of the crystallization and hardening behavior is required. The buildup of semi-crystalline domains leads to strong thickening, which shows similar behavioral patterns to suspensions of rigid, potentially interacting particles in a viscoelastic fluid. Early studies by Pogodina and Winter[19–21] revealed a gelation-like transition during polymer crystallization. The suspension-like hardening behavior of crystallizing polymer melts was further described by Lamberti et al.[22,23] and Pantani et al.,[24] and incorporated into a hardening model by Roozemond et al.[25] However, the detailed physics behind this process still remain a subject of debate. Due to the extremely high temperature-dependence of polymer crystallization, the correlation of data on the evolving crystallinity and flow behavior from separate instruments (e.g., DSC and rheology) is very difficult to achieve practically. In situ techniques such as low-field Rheo-NMR measure polymer crystallinity and flow properties simultaneously, leading to a substantially better online correlation of the data with the additional benefit of being able to study crystallization while applying well-defined shear protocols.

In terms of fundamental polymer science, a fully conclusive picture of the mechanism behind polymer crystallization is still missing. Especially for material systems and crystallization conditions that are more complex (flow, pressure, blends, additives, etc.), a detailed understanding of the interplay between local molecular dynamics, the structural buildup at the mesoscale, and macroscopic material properties is needed in order to clarify the mechanism of polymer crystallization.

In all of the aspects discussed above, new characterization techniques will help to achieve better insight into structure–property relationships and their underlying mechanisms, and ultimately lead to higher quality new or recycled products. In combination with computer simulations combined techniques will be the key to either prove or disprove the concepts under discussion, and they will also be beneficial in the controlled design of semi-crystalline materials and process conditions.

Dr. V. Räntzsch, M. B. Özen, Dr. K.-F. Ratzsch, Prof. G. Guthausen, Prof. M. Wilhelm
Karlsruhe Institute of Technology
76131 Karlsruhe, Germany
E-mail: Manfred.Wilhelm@kit.edu
Dr. E. Stellamanns, Dr. M. Sprung
German Electron Synchrotron
22607 Hamburg, Germany
The ORCID identification number(s) for the author(s) of this article can be found under https://doi.org/10.1002/mame.201800586.

DOI: 10.1002/mame.201800586

2. Hyphenated Rheology Techniques

In order to further understand the process of polymer crystallization, knowledge on the relationships between local molecular dynamics, structural buildup, and macroscopic material behavior under quiescent and flow conditions is required. For this task, hyphenated rheology techniques are powerful analytical tools as they combine information on the macroscopic flow and deformation behavior of soft matter with insights into structural and dynamic features on multiple length and time scales. Furthermore, they can be used to change the state of the material, permitting the study of polymer crystallization under well-defined flow conditions. The concept of hyphenation, that is, the coupling of different experimental techniques, has the advantage of simultaneous measurements resulting in the potential to identify correlations between two experimental techniques that are otherwise not easily accessible (**Figure 2**). The proper correlation of data from separate instruments is oftentimes difficult to achieve due to inherent small differences in the experimental conditions depending on sample size, shape, and experimental design. This is especially true for very temperature-sensitive processes such as polymer crystallization, for which the correlation of data from standalone instruments oftentimes leads to inconclusive results.[22] Temperature distributions across the sample space, actual cooling and heating rates, and sample dimensions differ depending on the technique used, for example, rheometers, calorimeters, spectrometers, optical microscopes, or scattering instruments. Correlated information obtained using hyphenated rheology techniques, on the other hand, is more precise, as a single sample is investigated at the same time using multiple techniques under identical conditions. The data can be analyzed quantitatively, providing a substantial gain in knowledge that will help to elucidate the mechanism of polymer crystallization, the hardening behavior, and the interplay between molecular features and the buildup of semi-crystalline morphologies.

There are three main types of hyphenated rheology techniques that are designed to characterize a) sample morphology, b) chemical structure, or c) molecular dynamics while performing rheological experiments. Rheo-Optics/-Microscopy combinations form a large group, which are mostly based on visible light sources.[26–29] Closely related are tomography set-ups using nuclear magnetic resonance (NMR)[30–36] as well as scattering techniques based on X-rays (SAXS, WAXS)[37–44] or neutrons (SANS).[45–48] Hyphenations of rheology and spectroscopy techniques are employed to obtain in situ information on the chemical structure of polymers, liquid crystals, or fats during chemical reactions, gelation, or crystallization while monitoring their rheological behavior. These set-ups are based on IR spectroscopy,[49–52] Raman spectroscopy,[53–56] or NMR spectroscopy.[57–62] Techniques that characterize molecular dynamics and consequently probe local molecular conformations were also combined with rheology. These set-ups are based on dielectric spectroscopy[63–67] and NMR relaxometry,[68–71] and can be used to investigate the origins of macroscopic flow behavior in soft matter. Further hyphenated rheology techniques that do not belong to any of the three main categories listed above are based on calorimetry,[72–75] dilatometry,[76–78] or electrical conductivity.[79] In the following, we discuss hyphenated set-ups based on state-of-the-art rheometers and in situ NMR relaxometry, small angle X-ray scattering (SAXS), and optical microscopy as these were selected in this study to perform studies on the relationships between the macroscopic flow behavior,

Volker Räntzsch received his Diploma (2013) and Ph.D. (2018) from the Karlsruhe Institute of Technology (KIT), Germany, where he studied the characterization of semi-crystalline polymers under the supervision of Prof. M. Wilhelm and Prof. G. Guthausen. In 2014, he visited Prof. J. Reynold's group at the Georgia Institute of Technology, USA, and worked on blends of conducting polymers. He joined Novolen Technology in the Fall of 2018 to continue his work on the development and application of polymeric materials.

Eric Stellamanns received his Diploma (2005) from the Technical University Braunschweig/Helmholtz Centre for Infection Research (HZI), Germany, and his Ph.D. (2011) from the Max Planck Institute for Dynamics and Self-Organization in Göttingen, Germany, under the supervision of Prof. T. Pfohl. He then joined the German Electron Synchrotron (DESY) and is working on the characterization of soft matter using methods of X-ray scattering and optical microscopy at beam line P10 of the PETRA III storage ring.

Manfred Wilhelm got his Diploma (1992) and Ph.D. (1995) from the Max-Planck-Institute for Polymer Research in Mainz, Germany, under the supervision of Prof. H. W. Spiess and worked with Prof. M. A. Winnik (University of Toronto, Canada), Prof. B. F. Chmelka (University of California Santa Barbara, USA), and Prof. J. Klein (Weizmann Institute, Israel). In 1997, he became an assistant professor at the MPI in Mainz (Reimund Stadler prize 1999), and was appointed associated professor at the Technical University Darmstadt in 2004. Since 2006, he is a tenured full professor at the Karlsruhe Institute of Technology (KIT).

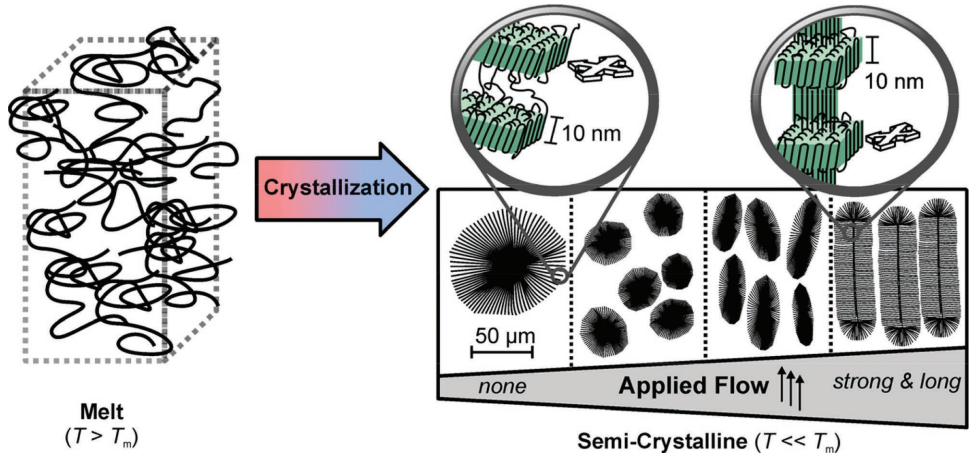

Figure 1. The morphology of semi-crystalline polymers depends on the duration and strength of the applied flow. For short and mild conditions an increase in nucleation density is observed. With increasing flow strength and duration, the spherulites become ellipsoidal, and for strong and long flow conditions, row-nucleated morphologies are obtained.

molecular dynamics, nano-scale morphology, and microstructure of crystallizing polymers (**Figure 3**).

2.1. Low-Field Rheo-NMR

The flow and deformation behavior of polymer melts can be thoroughly studied using rheology, whereas low-field NMR relaxometry (also called Time Domain (TD)-NMR) is a powerful technique for the characterization of molecular dynamics in polymeric materials.[80–85] To achieve a substantial insight into the interplay of these domains, especially under flow, these two methods were combined into a single set-up (Figure 3a).[71] This approach is different from other Rheo-NMR set-ups, as its main purpose is the study of molecular dynamics rather than chemical structure via NMR spectroscopy or morphology via magnetic resonance imaging. Low-field Rheo-NMR can be used to study processes with changes in the molecular dynamics and macroscopic flow behavior such as the curing of resins, the cross-linking of rubbers, or the crystallization of soft matter.[68,69,86,87] Based on the changes in molecular dynamics, a compositional analysis of multiphase soft matter systems during start-up and continued application of linear and nonlinear shear deformations can be obtained.[85] Furthermore, the effect of flow on the molecular dynamics of, for example, polymeric materials can be investigated making it a valuable tool to confirm certain concepts of polymer physics.

2.2. Rheo-SAXS

Investigating the X-ray scattering of soft matter under flow conditions has been of high interest for several decades, since changes in the nano-scale morphology are oftentimes strongly connected with desired properties such as the tensile strength of fibers, the long-range ordering of block copolymers, or the optical properties of liquid crystals. Time-resolved experiments of phase transitions and

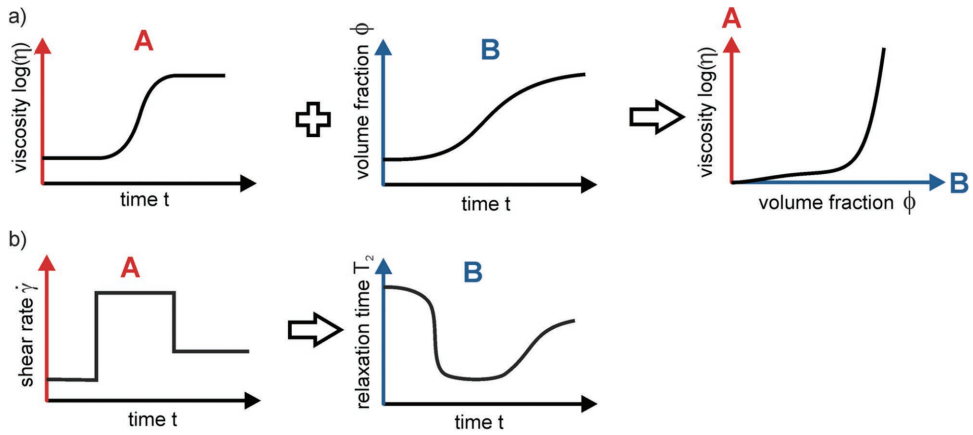

Figure 2. Examples of hyphenated rheological experiments: a) Correlated simultaneously acquired sets of data A and B for an arbitrary crystallization process. b) Effect of a change in parameter A on parameter B for an arbitrary shear-thinning material.

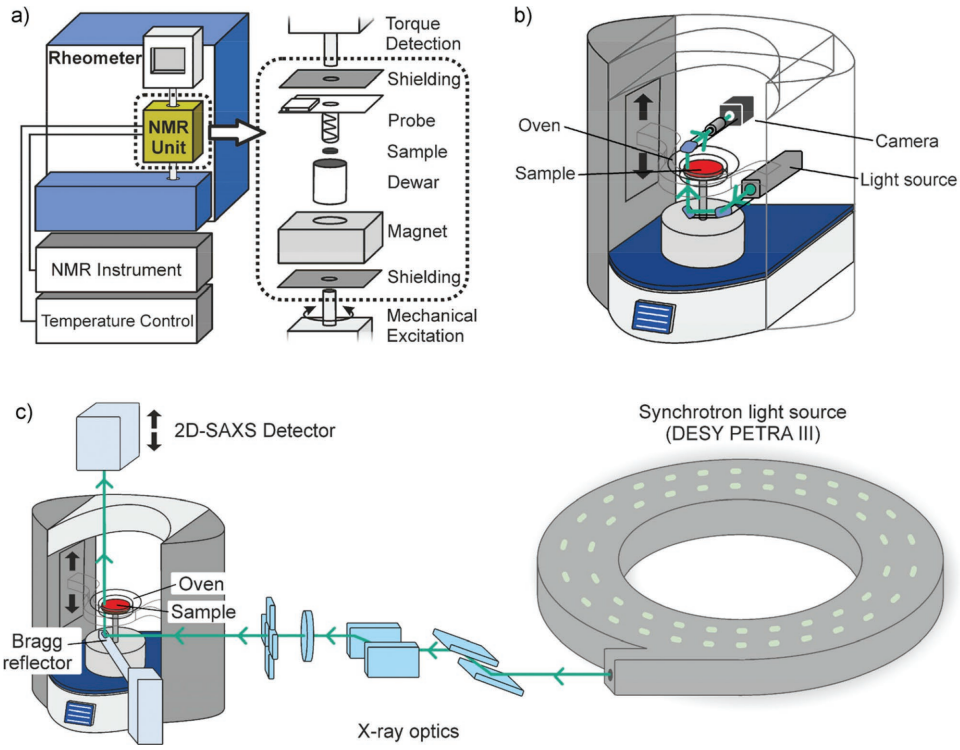

Figure 3. a) Low-field Rheo-NMR set-up based on a portable ^{1}H time domain (TD)-NMR unit (30 MHz) implemented in a strain-controlled shear rheometer (TA ARES). b) Rheo-Microscopy set-up based on a Thermo Haake MARS II rheometer. c) Rheo-SAXS set-up based on a Thermo Haake MARS II rheometer implemented into the beam path of beam line P10 at the German Electron Synchrotron (DESY). See Supporting Information for photographs of the respective set-ups.

ordering processes can usually only be performed using synchrotron radiation to achieve the high photon flux necessary for a time resolution on a millisecond to second scale. Early hyphenated set-ups were based on flow cells that allowed for the application of steady shear protocols in combination with wide and SAXS. Investigations were conducted on, for example, liquid crystals,[88,89] copolymers,[37,39,40] and semi-crystalline polymers.[38,90–96] More recently, slit flow experiments on crystallizing polymers based on multipass rheometers were conducted.[97–100] The structure formation during polymer processing methods such as extrusion,[14] film blowing,[101] and fiber spinning[102–104] was investigated using the respective hyphenated set-ups. Despite the insights into the structural buildup during quiescent and flow-induced crystallization of polymers, these studies lacked information on the evolving rheological behavior of the materials under study. Hyphenated set-ups that allowed for simultaneous measurements of rheology and X-ray scattering based on shear rheometers were realized by Panine et al.[105] who studied liquid crystals and polymer lattices, by Polushkin et al.[41,106] who developed a tooth geometry to study the alignment of block copolymers, by Pfleiderer et al.[107] who built a set-up that allowed for X-ray scattering studies of fluids in the vorticity direction, and by Struth et al.[42,44,69] who developed a hyphenated set-up based on a stress-controlled rheometer with a vertical beam path for the study of low to highly viscous samples (Figure 3c). The latter set-up was used in the experiments presented here, and furthermore by other researchers to study block copolymers,[43,67,108] platelet dispersions,[109] and colloidal systems.[110,111] Recently, hyphenations of extensional rheometers and X-ray scattering techniques were used by Yan et al.,[112] Liu et al.,[113] and Wingstrand et al.[10] to reveal the interplay of structural buildup and elongation rheology during flow-induced polymer crystallization.

2.3. Rheo-Microscopy

Rheo-optical set-ups based on the scattering/absorption of visible light or microscopy (Figure 3b) in combination with flow cells and rheometers have been extensively used in the past to study soft matter. Reviews of different rheo-optical set-ups and their applications were published by, for example, Fuller[27] and Wagner.[28] Simultaneous investigations on the microstructure and rheology were performed on suspensions,[114,115] emulsions,[116,117] and liquid crystals.[26,118,119] Furthermore, experiments on amorphous polymeric material systems such as polymer solutions,[120–123] block copolymers,[124,125] and polymer melts[126,127] were carried out to investigate the effects of flow on the conformation of polymeric chains. The structural buildup of semi-crystalline polymers under quiescent crystallization conditions was studied to investigate the relationship between the microstructure and hardening behavior of crystallizing polymers by, for example, Pogodina et al.,[20,21] Elmoumni et al.,[128]

and Pantani et al.[24] Flow-induced crystallization was studied by numerous groups using rheo-optical methods and some selected references are discussed in the following. Pioneering works were carried out by Keller and Mackley who developed a multipass rheometer with in situ microstructural characterization and studied crystallizing polymers under process-like conditions.[11,129–133] Winter et al. investigated the molecular-weight dependence of flow-induced crystallization.[134,135] More recently, Pantani et al. studied the kinetics of crystallizing polymers under flow conditions using Rheo-Microscopy.[136–138] Further studies were carried out by Koscher and Fulchiron[139] and Housmans et al.[140] who aimed for experimental evidence to validate theoretical models of flow-induced crystallization.

3. Experimental Section

3.1. Apparatuses

The hyphenated low-field Rheo-NMR set-up is based on a portable ^{1}H NMR unit (B_0 = 0.7 T, $\omega_L/2\pi$ = 30 MHz for ^{1}H) that was integrated into a commercial strain-controlled TA/Rheometrics ARES shear rheometer (Figure 3a).[71] The NMR magnet consists of a Halbach array of 92 NdFeB permanent magnets with a Dewar between the temperature-sensitive permanent magnets and the sample space to achieve good thermal insulation. The sample temperature could be controlled from −15 to +210 °C using a convective heating system and a Bruker Variable Temperature unit. The broadband NMR probe used in these experiments is based on a parallel tank circuit equipped with a solenoid coil (l = 33 mm, d = 16 mm) and two capacitors (match & tune) exhibiting a dead time of 12 µs and pulse lengths of 3 µs (90°) and 6 µs (180°) at 0 dB pulse attenuation, respectively. Pulsing, data acquisition, and processing were performed by a Bruker "the minispec" electronic unit. Proton-free and non-conducting rheological geometries were made from ceramics (13 mm parallel-plate).

The hyphenated RheoSAXS setup was developed by the groups of Prof. Wilhelm (KIT) and B. Struth (DESY) in close collaboration with Thermo Scientific (Figure 3c).[42,44,69] A unique feature of this set-up is that the incident X-ray beam is reflected by a Ge(333) crystal in order to maintain the horizontal shear flow direction of the used Haake MARS II rheometer (Thermo Scientific, Karlsruhe, Germany). The rheometer motor was flipped and assembled at the lower part of the instrument ("inverted rheometer") to open up the top space for the beam path and the Pilatus 300k 2D-SAXS detector (Dectris, Baden-Dättwil, Switzerland). All experiments reported here were performed on the new RheoX end station installed at beamline P10 of PETRA III. The q-range of the instrument is 0.02 to 4 Å^{-1} at a wavelength of λ = 1.54 Å. The sample environment was developed in-house to allow for measurements at temperatures of +25 to +300 °C under an inert nitrogen atmosphere. Parallel-plate geometries (35 mm) with X-ray transmissive windows were made from polyimide.

The hyphenated Rheo-Microscopy set-up shown in Figure 3b was again based on the inverted stress-controlled Haake MARS II rheometer (Thermo Scientific, Karlsruhe, Germany) with the sample environment that was also used for the Rheo-SAXS set-up. The rheometer was equipped with 35 mm parallel-plate geometries made from glass. The home-built optical microscopy unit consisted of a polarized white LED light source, an objective (achromatic triplet f = 16 mm), tubus lenses (achromatic doublets: f = 10 and 100 mm), and a 12-bit monochrome digital camera with a 1936 × 1216 px, 1/1.2″ CMOS chip (IDS Imaging Development Systems GmbH, Obersulm, Germany). Due to the open geometry of the inverted Haake MARS II rheometer, it is possible to conduct rheology experiments, SAXS/WAXS, and high resolution microscopy simultaneously using quartz plate geometries with diamond windows.

3.2. Materials and Procedures

Quiescent and flow-induced crystallization of isotactic polypropylene was studied under isothermal conditions over a temperature interval of 130–140 °C. The main material of investigation was a Ziegler–Natta polypropylene i-PP-1 (M_w = 246 kg mol^{-1}, $Đ$ = 2.7, *mmmm* = 94%, PP070G2M, Repsol, Spain). Prior to all crystallization experiments, the polypropylene samples were melted at 200 °C for 15 min to erase the thermal history. All polymer crystallizations were monitored by rheological time sweeps with low shear strain amplitude γ_0 = 0.5% and angular frequency ω = 1 rad s^{-1} to detect the change in flow behavior without disturbing crystal formation. For all flow-induced crystallizations, a steady shear step was started right after the desired crystallization temperature was reached.

For Rheo-NMR, the changes in molecular dynamics and the buildup of crystallinity from an isotropic melt were monitored by ^{1}H NMR relaxometry using a combined MSE-CPMG pulse sequence.[81,85] The mass crystallinity $X_c(t)$ was converted into a volume fraction $\phi_c(t)$ using the densities of a fully amorphous and a theoretically 100% crystalline sample.[141]

For Rheo-SAXS, the X-ray beam (250 × 250 µm) was positioned at r = 14 mm of the 35 mm parallel-plate geometries. All 2D-SAXS patterns were acquired over 5 s. Upon complete crystallization, the morphologies were analyzed using ex situ scanning electron microscopy (SEM). The samples were etched with an acidic permanganate solution (0.2 mol l^{-1} $KMnO_4$ in 10 : 4 : 1 H_2SO_4 (96%), o-H_3PO_4 (85%), H_2O for 2 h at RT with subsequent washing using H_2O_2 (30%)/H_2O and sonication for 30 min in acetone). A 2 nm thick coating of Pt was deposited onto the specimens using a Leica EM ACE 600 sputter coater. SEM images were taken using a Zeiss Gemini/LEO 1530 system with an accelerating voltage of 5 kV and a 30/60 µm aperture.

For Rheo-Microscopy, the observation window was at r = 14 mm as in the Rheo-SAXS experiments. The sample thickness was adjusted to 200–250 µm to monitor the growth of individual spherulites. All micrographs were acquired in monochrome mode and under non-cross polarized conditions to observe the flowing polymer melt prior to crystallization.

4. Results and Discussion

4.1. Interplay between Molecular Dynamics and Rheology in Crystallizing Polymers: Rheo-NMR

The temperature-dependence of isothermal polymer crystallization was investigated by simultaneously monitoring the rheological behavior and the emerging relative polymer crystallinity via NMR. In **Figure 4**, the time evolution of the absolute complex viscosities $|\eta^*| = \sqrt{(G')^2 + (G'')^2}/\omega$ (G': storage modulus, G'': loss modulus) and relative crystallinities ϕ_c/ϕ_c^∞ is shown for the investigated isotactic polypropylene (i-PP). The sensitivity of crystallization toward temperature is high over the chosen interval: a decrease of 2 K led to a two times faster crystallization as detected by the half times. The trend of faster crystallization with decreasing crystallization temperature for $T_{cryst} > (T_m^0 + T_g)/2$ assuming a symmetric growth rate distribution was well resolved by both techniques.

To further evaluate the data, all crystallinity curves were directly modeled using an Avrami model up to $\phi_c/\phi_c^\infty = 0.5$ to facilitate the correlation of rheological parameters with polymer crystallinity from NMR relaxometry (**Table 1**):[142]

$$\frac{\phi_c}{\phi_c^\infty} = 1 - \exp\{-[K(t-t_0)]^n\} \quad \text{(Avrami model)} \tag{1}$$

Table 1. Parameters obtained from an Avrami model fit to the data shown in Figure 4b and from an Extended Einstein model fit to the data of Figure 5.

T_{cryst} [°C]	K [min^{-1}]	n	t_0 [min]	D	C
130	0.18	2.5	8.5	29×10^3	4.1
132	0.11	2.4	9	44×10^3	4.6
134	0.069	2.5	10	46×10^3	5.0
136	0.045	2.6	11	58×10^3	5.1

By plotting a normalized rheological function, for example, the reduced absolute complex viscosity $|\eta^*|/|\eta^*|_0$, as a function of relative crystallinity ϕ_c/ϕ_c^∞(= the degree of space filling φ), the effect of temperature on polymer crystallization is mostly removed (**Figure 5**, see Supporting Information for additional correlation plots).[22]

In Figure 5, a higher viscosity was observed at lower crystallization temperatures before the curves merged to form a single line. A strong relative increase in viscosity occurred at degrees of space filling below 10–15%, which indicated some form of long-range interactions between the growing spherulites. As the correlation plots were similar to those of solid-particle suspensions, they were evaluated using suspension and semi-empirical models:[143,144]

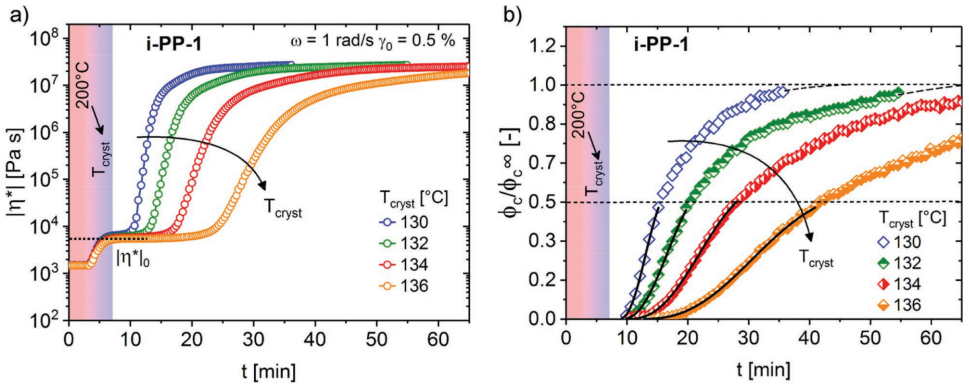

Figure 4. a) Simultaneously acquired absolute complex viscosity $|\eta^*|$ and b) relative crystallinities ϕ_c/ϕ_c^∞ during isothermal crystallization of isotactic polypropylene (i-PP) from the melt using a hyphenated low-field Rheo-NMR set-up. Black lines: Avrami model fits based on Equation (1).

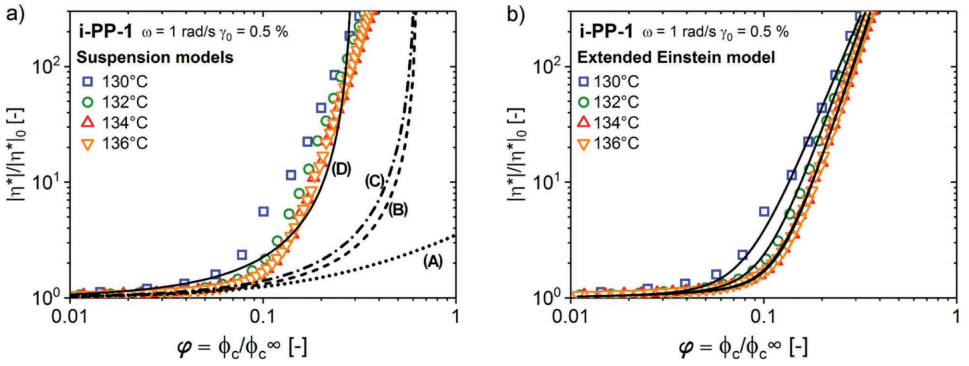

Figure 5. Reduced absolute complex viscosity as a function of relative crystallinity ϕ_c/ϕ_c^∞ (= the degree of space filling φ) for the temperature series of Figure 4. a) Suspension models: Einstein (A), Krieger–Dougherty with $\varphi_{max} = 64\%$ (B), Quemada with $\varphi_{max} = 64\%$ (C), Quemada with $\varphi_{max} = 30\%$ (D). b) Semi-empirical extended Einstein model based on Equation (5) (determined parameters shown in Table 1).

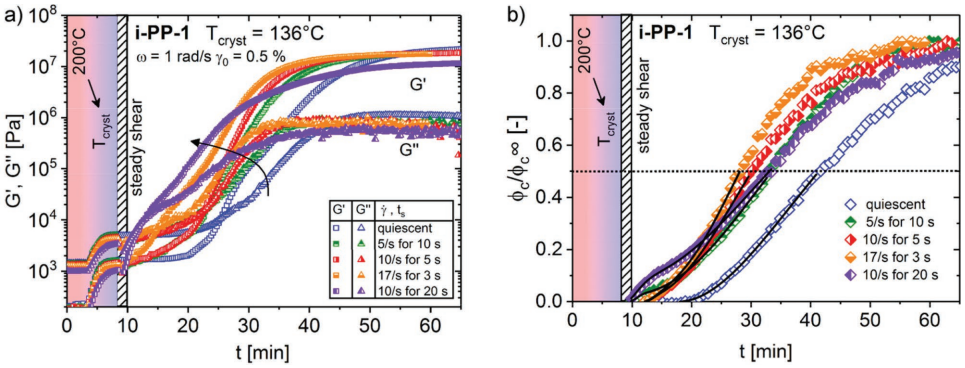

Figure 6. a) Simultaneously acquired moduli G', G'' and b) relative crystallinities ϕ_c/ϕ_c^∞ during flow-induced crystallization of i-PP-1 at 136 °C. Upon cooling, different steady shear protocols were applied, which either had a similar total shear strain or shear rate. A substantial increase in the speed at which G', G'', and ϕ_c/ϕ_c^∞ developed was observed for all experiments, which followed the trend "higher shear rate and longer duration lead to faster crystallization".

$$\frac{\eta}{\eta_0} = 1 + 2.5\varphi \quad \text{(Einstein)} \tag{2}$$

$$\frac{\eta}{\eta_0} = \left[1 - \frac{\varphi}{\varphi_{max}}\right]^{-2.5\varphi_{max}} \quad \text{(Krieger-Dougherty)} \tag{3}$$

$$\frac{\eta}{\eta_0} = \left[1 - \frac{\varphi}{\varphi_{max}}\right]^{-2} \quad \text{(Quemada)} \tag{4}$$

$$\frac{\eta}{\eta_0} = 1 + 2.5\varphi + D\varphi^c \quad \text{(Extended Einstein)} \tag{5}$$

The Einstein model is known to be valid only for very dilute systems of monodisperse spheres. Consequently, it only provided a good fit at small values of $\varphi < 0.05$, but did not describe the steep increase observed at $\varphi \approx 0.1$ as shown in Figure 5. Using a maximum packing fraction of $\varphi_{max} = 64\%$, which is usually assumed for hard sphere suspensions,[143] the Krieger–Dougherty and Quemada models did not match the experimental data. A better description was achieved when the Quemada equation was modified by assuming a maximum packing fraction of $\varphi_{max} = 30\%$ (Figure 5, curve 4). The best fit was achieved using a combination of the Einstein model and a power law (extended Einstein model, Equation (5), Figure 5b). With only two free parameters, this semi-empirical model describes the transition from the dilute suspension regime (Einstein) to the physical gel state (power law). Parameter D represents the dynamic range of $|\eta^*|/|\eta^*|_0$ over the modeled interval, whereas C is potentially associated with the coordination number of interacting spherulites (Table 1).

Besides measuring the evolution of the flow behavior and crystallinity simultaneously during quiescent crystallization, one can also impose a pre-shear state prior to crystallization using short-term steady shear protocols of varying shear rate, shear strain, and duration. Flow is known to have a strong effect on the crystallization kinetics, the morphology, and material properties of semi-crystalline polymers as described in the introduction. To separate the effects of flow and crystallization temperature, the short-term shear protocol by Janeschitz-Kriegl and coworkers was employed in the following experiments (rapid cooling to T_{cryst}; short application of steady shear during the induction time; monitoring of the effects on crystallization).[12] In **Figure 6**, experimental results for flow-induced crystallizations at $T_{cryst} \approx 136$ °C are shown where the steady shear protocols were selected to have either a similar total shear strain ($\gamma \approx 50$) or a similar shear rate ($\dot{\gamma} \approx 10\ s^{-1}$). All pre-sheared melts showed a significantly faster crystallization, which was seen in the moduli G' and G'' as well as in the relative crystallinity ϕ_c/ϕ_c^∞. For the two samples exposed to the highest shear rate ($\dot{\gamma} = 17\ s^{-1}$ for 3 s, $\gamma \approx 50$) and total shear strain ($\dot{\gamma} = 10\ s^{-1}$ for 20 s, $\gamma \approx 200$), the curves exhibited an almost immediate increase in the moduli G', G'' and the relative crystallinity ϕ_c/ϕ_c^∞ after the cessation of flow. Even though the applied shear rate was lower in the "10 s^{-1} for 20 s" experiment, it showed the fastest crystallization and earliest rise in the moduli G' and G''. Hence, the higher total shear strain and the associated shearing time t_s seemed to compensate for the lower shear rate. The immediate increase in moduli and crystallinity suggested that not only the overall speed was affected, but that changes in the morphology of the crystallizing polymer occurred. As the relaxation times of the high molecular-weight tail were on the order of seconds at the chosen temperature, certain chain orientation and stretch was induced (Weissenberg number $Wi = \dot{\gamma}\lambda \gg 1$). Indeed, the presence of row-nucleated

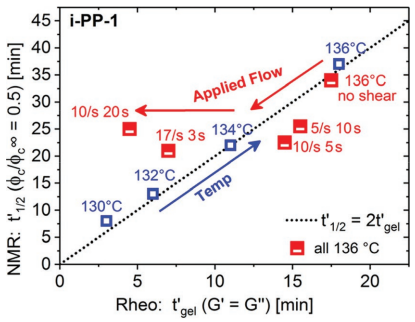

Figure 7. Crystallization half times $t'_{1/2}$ as a function of the crossover times t'_{gel} at different crystallization temperatures (open squares) and pre-shear conditions (semi-filled squares). In the upper right, two quiescent experiments performed at 136 °C are shown as a measure of repeatability.

structures and a high nucleation density was confirmed later by ex situ SEM.

To further compare the flow-induced crystallization experiments, crystallization half times $t'_{1/2}$ for $\phi_c/\phi_c^{\infty} = 0.5$ were plotted against the corresponding rheological crossover times t'_{gel} for $G' = G''$ as shown in **Figure 7**. The relationship between $t'_{1/2}$ and t'_{gel} was well described by the proportionality $t'_{1/2} \approx 2t'_{gel}$ (dotted line) for all investigated temperatures of the quiescent crystallization experiments of Figure 6. In case of the the pre-sheared experiments, a shift to lower times was observed for moderate shearing conditions, which was similar to the behavior found at a lower crystallization temperature. At higher shear rates and total shear strains, the times t'_{gel} decreased further and the crystallization half times $t'_{1/2}$ remained practically constant within the experimental uncertainty. The shorter time needed to achieve a gel state at higher shear rates and longer shear durations might be a consequence of increased nucleation and the influence of anisotropic row-nucleated structures.

4.2. Correlating Nano-Scale Morphology and Rheology of Crystallizing Polymers: Rheo-SAXS

Applying flow during polymer crystallization is known to alter the semi-crystalline morphology as discussed in the introduction. Again, the short-term shear protocol developed by Janeschitz-Kriegl and coworkers was applied to study the effects of flow independently from the chosen crystallization temperature.[12] In **Figure 8**, the rheological moduli G' and G'' are plotted together with selected simultaneously acquired 2D-SAXS patterns. With increasing maximum shear rate, a speed-up of crystallization was detected by the rheological parameters (the applied shear rates were gradually increased during the steady shear interval up to the maximum values. See Supporting Information.). All experiments under flow conditions exhibited dumbbell-shaped 2D-SAXS patterns, indicating the formation of anisotropic structures perpendicular to the flow direction. The associated q values were on the order of 0.02 Å^{-1}, corresponding to a long spacing $d \approx 30$ nm. Thus, the observed patterns were likely caused by lamellae that grew perpendicular to the flow direction.

The flow-induced anisotropy during polymer crystallization as detected by the 2D-SAXS patterns was further analyzed using Herman's orientation function:[145,146]

$$F_H = \frac{3\langle\cos^2\alpha\rangle - 1}{2} \quad (6)$$

F_H: orientation parameter, $\alpha = \chi - 90°$: orientation vector with respect to the flow direction.

Equation (6) was initially employed to describe the degree of orientation in drawn fibers by measuring their birefringence. As the periodicity of orientation is 180°, the second Legendre polynomial was chosen by Herman to obtain a quantitative measure of orientation. The average intensity term $\langle\cos^2\alpha\rangle$ is given by the fraction of two sinα-weighted integrals:

$$\langle\cos^2\alpha\rangle = \frac{\int I(\alpha)\cos^2\alpha \sin\alpha \, d\alpha}{\int I(\alpha)\sin\alpha \, d\alpha} \quad (7)$$

In **Figure 9**a, the obtained orientation parameters F_H for the crystallization experiments of i-PP-1 under different conditions are plotted as a function of time. The experiment with a maximum shear rate of 8 s^{-1} showed a maximum in F_H at approximately 25 min that decreased only slightly over time compared to the other experiments. The final degree of orientation upon complete crystallization was $F_{H,final}(8\ s^{-1}) \approx 0.24$, whereas the data

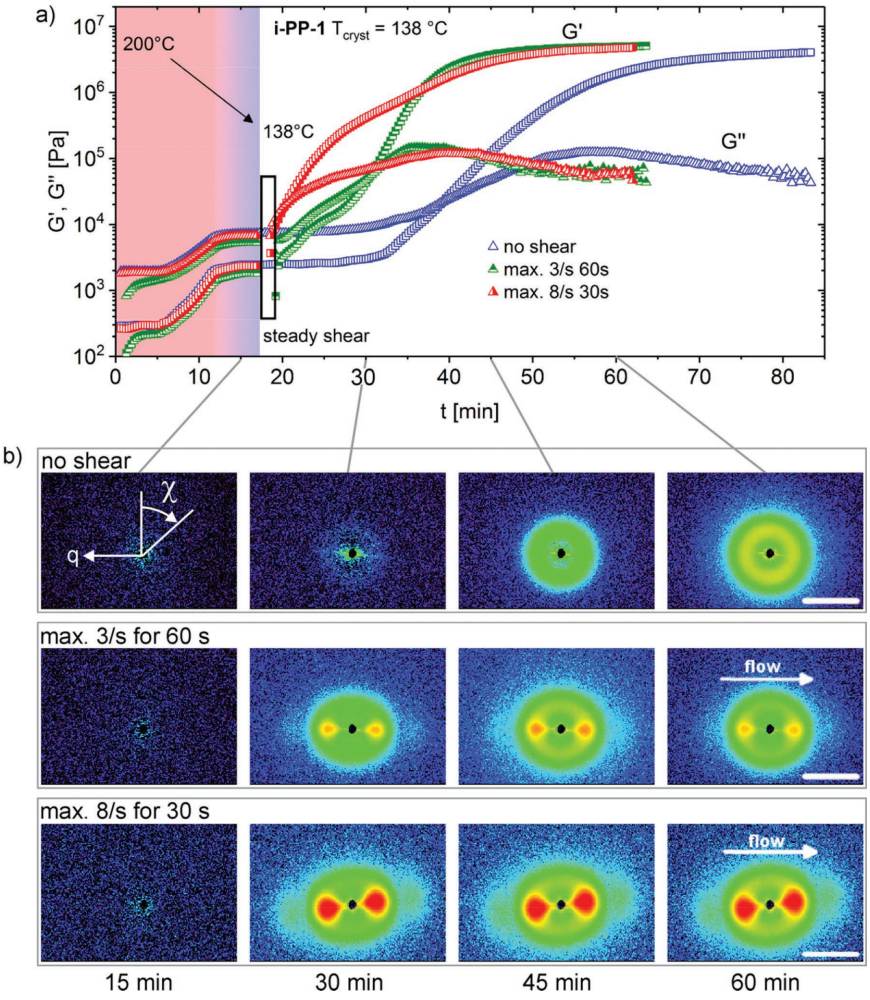

Figure 8. a) Simultaneously acquired moduli G', G'' and b) selected 2D-SAXS patterns for crystallizations of i-PP-1 under quiescent and flow conditions using a hyphenated Rheo-SAXS set-up. A speed-up of the crystallization with increasing maximum shear rate was detected by the rheological parameters. The 2D-SAXS data showed the formation of dumbbell-shaped patterns with long spacings of d ≈ 30 nm. Image at 15 min subtracted, scale bar: 0.05 Å^{-1}.

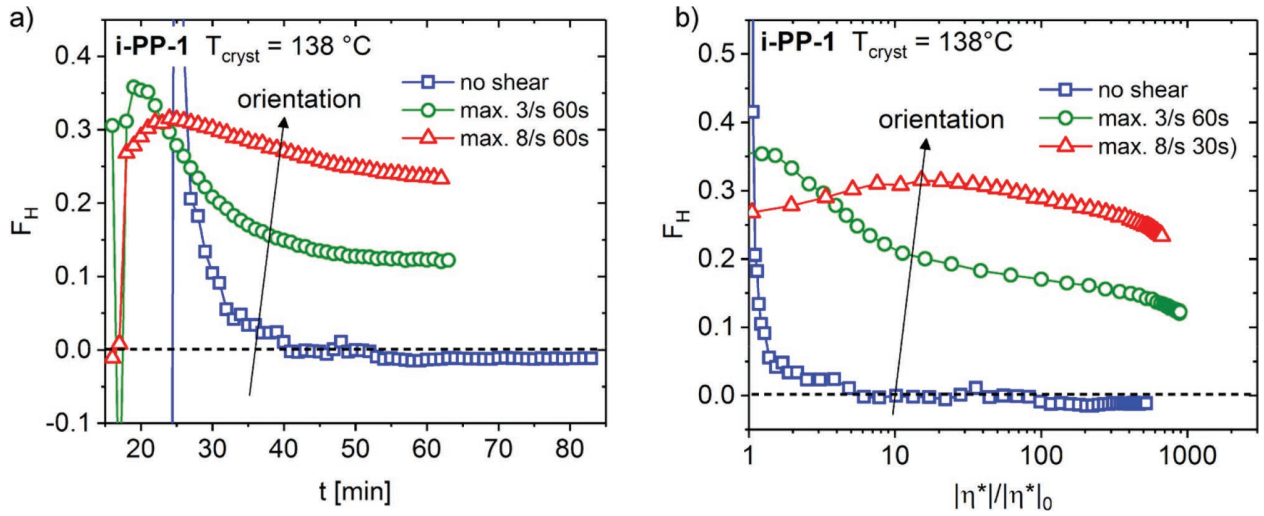

Figure 9. a) Herman's orientation parameter F_H versus time t and b) F_H versus the reduced absolute complex viscosity $|\eta^*|/|\eta^*|_0$ for crystallizations of i-PP-1 under quiescent and flow conditions.

for the experiment at a maximum shear rate of 3 s^{-1} showed that this parameter decreased to $F_{H,final}(3\ s^{-1}) \approx 0.12$, and, for the quiescent experiment, to $F_{H,final}(0\ s^{-1}) \approx 0$ as expected. In Figure 9b, it is seen that all obtained orientation parameters correlated with the reduced absolute complex viscosity. For $1 \leq |\eta^*|/|\eta^*|_0 \leq 10$, the experiment under quiescent conditions and the experiment at a maximum shear rate of 3 s^{-1} showed a rapid decrease in F_H, whereas for $10 \leq |\eta^*|/|\eta^*|_0 \leq 1000$ only a minor loss in orientation was detected. The data for the experiment at a maximum shear rate of 8 s^{-1} had a maximum at $|\eta^*|/|\eta^*|_0 \approx 10$, and then followed the decreasing trend seen in the other experiments at higher values of $|\eta^*|/|\eta^*|_0$. An experiment performed at a maximum shear rate of 5 s^{-1} (not shown) displayed a lower overall degree of orientation than the experiment with a maximum shear rate of 3 s^{-1}, which was potentially a consequence of the lower applied initial shear rates (see Supporting Information). All experiments including the one under quiescent conditions showed a high level of orientation over $t \approx 20$–30 min. Generally, even experiments under nominally quiescent conditions show some form of flow on a microscopic level due to convection and contraction upon cooling. Thus, the observed high degrees of orientation at the beginning of all crystallization processes likely originate from the alignment of anisotropic nuclei at the early stages of polymer crystallization. As a complementary technique to investigate the nano-scale morphology, ex situ SEM was carried out on the recovered specimen upon complete crystallization. All samples were

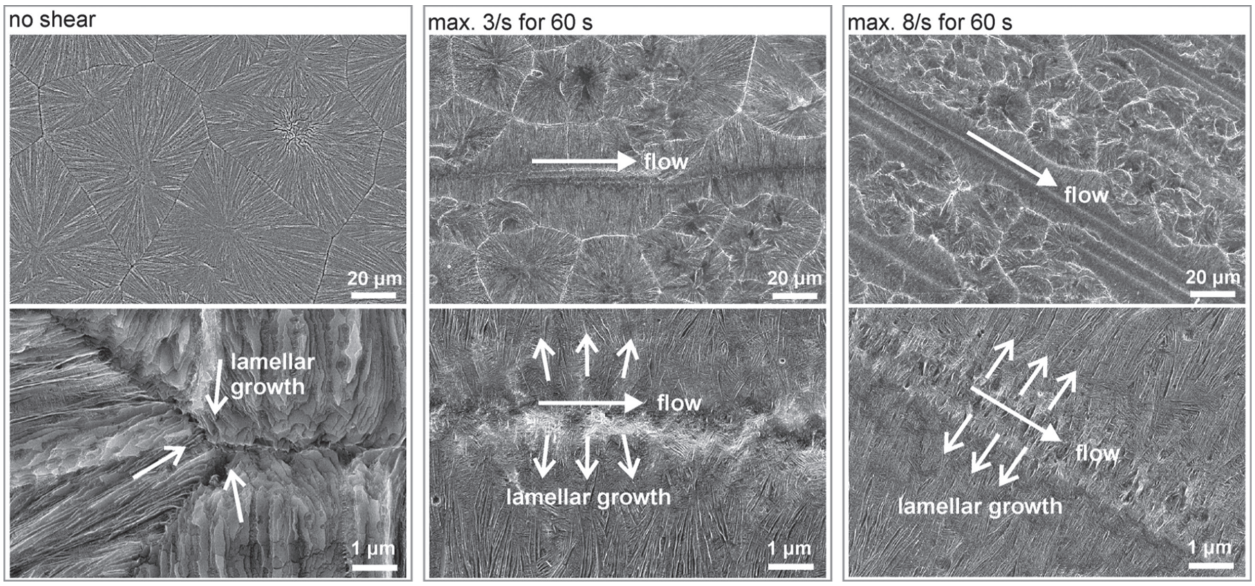

Figure 10. SEM images at different magnifications of etched i-PP-1 crystallized at 138 °C under quiescent and flow conditions.

etched prior to SEM using an acidic permanganate solution as described in the experimental section. The images were recorded at a position of 3 mm from the edge of the sample where the X-ray beam penetrated the material. The analysis of the sample with a maximum shear rate of 3 s^{-1} confirmed an increased nucleation density with spherulite sizes of 20–30 µm compared to the quiescently crystallized i-PP-1 sample (**Figure 10**). Furthermore a small number of elongated, but still spherulitic structures, were observed. The specimen from the experiment at a maximum shear rate of 8 s^{-1} showed the highest degree of anisotropy and a substantially increased nucleation density with spherulite sizes of 10–20 µm (Figure 10). Row-nucleated structures were found throughout the sample with a strong directional orientation of the grown lamellae perpendicular to the flow direction that most likely caused the observed 2D-SAXS patterns and rigidification in the early stages of crystallization.

4.3. Relationship between Microstructure and Rheology in Polymer Crystallization: Rheo-Microscopy

The crystallization of isotactic polypropylene was further studied using hyphenated Rheo-Microscopy (Figure 3). The evolution of the rheological moduli and simultaneously acquired micrographs for a quiescent crystallization of the Ziegler–Natta grade i-PP-1 at T_{cryst} = 138 °C is shown in **Figure 11**. Soon after the temperature was reached small nuclei formed that grew into larger spherulites over time. At this stage, the rheological moduli did not yet increase. For $t \geq 30$ min, the moduli G' and G'' displayed an increasing trend when grown spherulites occupied a substantial volume of the polymer melt. The crossover $G' = G''$ was reached shortly before 40 min and the micrographs showed a denser microstructure with increasing time. The short-term shear protocol by Janeschitz-Kriegl was again employed to study the effects of flow independently from the chosen crystallization temperature.[12] Stresses of 12 to 21 kPa were applied for 60 s using the stress-controlled Haake MARS II, which led to a practically instantaneous application of shear rates between $\dot{\gamma}$ = 1 to 3 s^{-1} and a linear increase in the total shear strain depending on the applied stress (see Supporting Information). An additional test that was carried out at 24 kPa showed delayed crystallization, which was most probably caused by sample slippage on the glass surfaces during steady shear due to the higher shear stress and was therefore excluded from further analysis. In Figure 11b, micrographs recorded at different points in time during the experiments of Figure 11a are shown. The microstructure of the 12 kPa ($\dot{\gamma}$ = 1 s^{-1}) experiment was relatively similar to its quiescent counterpart. However, at higher applied stresses and shear rates, a significantly higher nucleation density was observed.

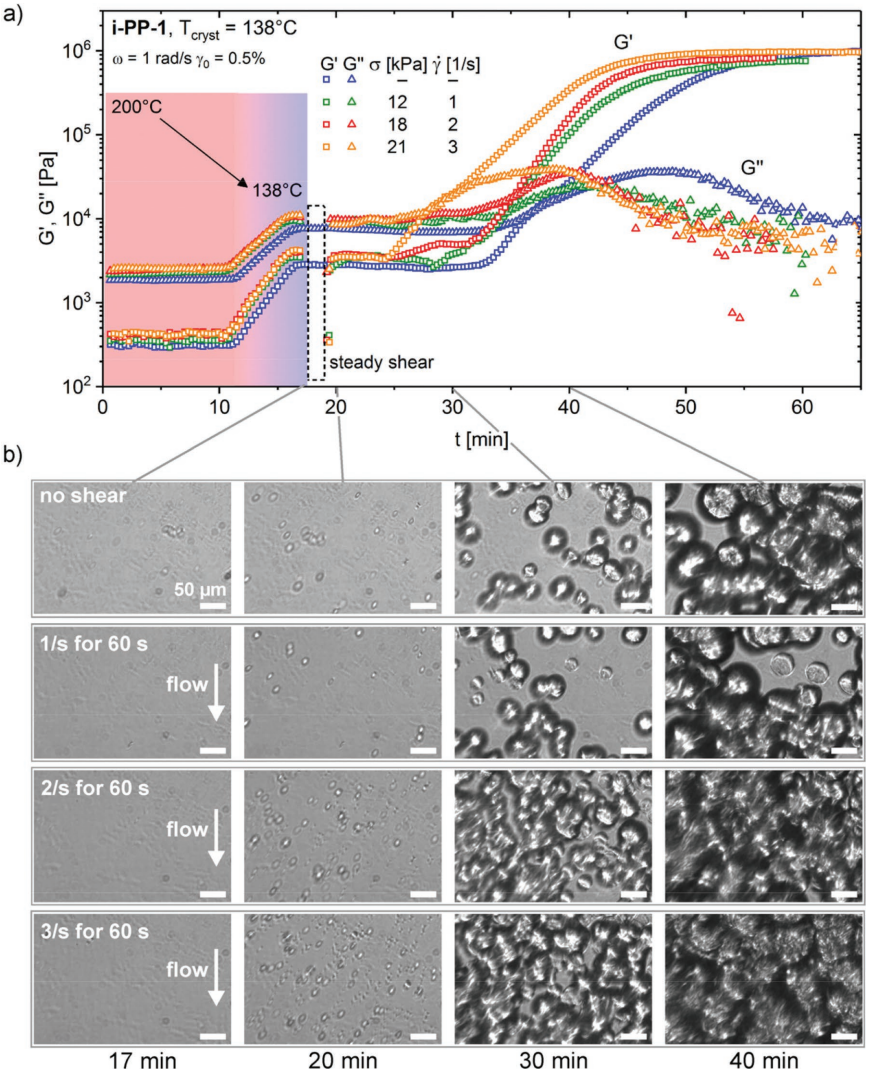

Figure 11. Simultaneously acquired a) rheological moduli and b) micrographs of i-PP-1 during quiescent and flow-induced crystallizations at $T_{cryst} \approx 138$ °C using hyphenated Rheo-Microscopy (scale bar: 50 µm, flow applied in the vertical direction).

In **Figure 12**, micrographs of the microstructure at the crossover of G' and G'' are shown for the different experimental conditions. For the 12 kPa ($\dot{\gamma}$ = 1 s^{-1}) experiment, a similar microstructure was observed as seen for the experiment under quiescent conditions. The experiments at higher applied stresses/shear rates showed significantly increased nucleation and an overall higher degree of space filling at the point of gelation. Notably, many nuclei were formed close to the surface of the glass plates under stronger flow conditions. This effect might be associated with a reduction in surface stresses caused by the growing nuclei. As the microstructure of strongly sheared samples becomes more heterogeneous, the micrographs shown in Figure 12 represent snapshots of the local microstructure at r = 14 mm. Thus, the degree of space

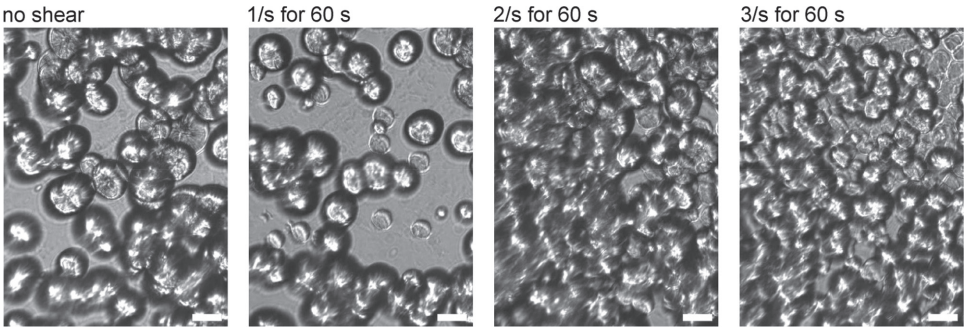

Figure 12. Micrographs recorded at the rheological crossover ($G' = G''$) for i-PP-1 crystallized at $T_{cryst} \approx 138$ °C under different conditions using hyphenated Rheo-Microscopy (scale bar: 50 µm, flow applied in the vertical direction).

filling φ was relatively high at the surfaces when the crossover of G' and G'' was detected.

For the quiescent experiment shown in Figure 12 (no shear), the degree of space filling φ at the crossover ($G' = G''$) was estimated by assuming a set of monodisperse spheres in a box of $600 \times 375 \times 250$ µm^3. Ninety spheres with $r \approx 30$ µm were detected where the 24 spheres at the edges were counted as half. The number of equivalent spheres $N \approx 78$ corresponded to a degree of space filling $\varphi \approx 16\% \pm 5$ %. The determined degree of space filling agreed well with the results obtained by Rheo-NMR for high crystallization temperatures and points toward a percolation phenomenon of the growing spherulites. Different from hard sphere suspensions, the spherulites of crystallizing polymers are likely interacting, that is, they impinge and form persisting rigid networks within the supercooled melt.

5. Conclusions

In this article, hyphenated techniques based on rheology and in situ NMR relaxometry, SAXS, and optical microscopy were presented as powerful tools for the study of soft matter. These combined set-ups allow for simultaneous 2D measurements and the application of flow profiles. They were applied to the study of polymer crystallization under quiescent and flow conditions and helped to reveal relationships between the molecular dynamics, morphology, and rheology of crystallizing polymers. The obtained results confirmed a physical gelation process during polymer crystallization mediated by the interaction of growing superstructures at volume fractions $\varphi \approx 10$ to 15%. The analysis of the hardening behavior with the help of rheological models showed a strong nonlinear relationship between the degree of space filling and the viscosity leading to a relative increase in viscosity by four orders of magnitude compared to the melt. The evolution of the morphology on the nano- and micro-scale during quiescent and flow-induced crystallizations was analyzed using Rheo-SAXS and optical Rheo-Microscopy. The increased nucleation densities and the formation of row-nucleated structures upon the application of flow were connected to the rheological behavior. Based on the experimental results, polymer crystallization from the melt most probably follows a nucleation and growth mechanism under the explored experimental conditions. The formation of row-nucleated structures during flow-induced crystallization is likely associated with the altered conformation of the longest polymer chains under the application of flow. Overall, the application of hyphenated rheology techniques to polymer crystallization helped to further clarify the hardening behavior during quiescent and flow-induced crystallization, the crystallization mechanism, and the formation of row-nucleated structures. Other soft materials such as crystallizing fats, colloids, or phase-separating polymers could be studied using the described characterization techniques. Despite the increased complexity and data analysis, hyphenated rheology techniques provide valuable correlated information on the relationships between rheological behavior, structure, and dynamics on different length and time scales. In the future, the presented set-ups could be further developed to include, for example, the application of process-like conditions, the use of more complex NMR pulse sequences, and the study of slow dynamics using coherent X-ray photon correlation spectroscopy (XPCS).

Supporting Information

Supporting Information is available from the Wiley Online Library or from the author.

Acknowledgements

The projects were funded by Deutsche Forschungsgemeinschaft (DFG, SPP1369-B10, Pro^{2}NMR) and by Bundesministerium für Bildung und Forschung (BMBF, 'FUNgraphen'). The authors thank V. Zibat (Laboratory for Electron Microscopy, KIT, Karlsruhe, Germany) for SEM imaging, Prof. A. J. Müller (University of the Basque Country, Donostia-San Sebastián, Spain) for providing the polypropylene grade and Dr. J. Kübel (KIT, Karlsruhe, Germany) for proofreading the manuscript. M.B.Ö. thanks the Ministry of National Education of the Republic of Turkey for financial support.

Conflict of Interest

The authors declare no conflict of interest.

Keywords

hyphenation, polymer crystallization, polypropylene, rheology, Rheo-microscopy, Rheo-NMR, Rheo-Optics, Rheo-SAXS

Received: October 3, 2018
Revised: November 27, 2018
Published online: December 13, 2018

[1] L. Mandelkern, "*Crystallization of Polymers: Volume 1, Equilibrium Concepts*", 2nd ed., Cambridge University Press, Cambridge, UK **2002**.
[2] L. Mandelkern, "*Crystallization of Polymers: Volume 2, Kinetics and Mechanisms*", 2nd ed., Cambridge University Press, Cambridge, UK **2004**.
[3] G. Reiter, G. R. Strobl, "*Progress in Understanding of Polymer Crystallization*", Springer, Berlin **2007**.
[4] E. Piorkowska, G. C. Rutledge, "*Handbook of Polymer Crystallization*", John Wiley & Sons, Hoboken **2013**.
[5] B. Monasse, J. Haudin, *Colloid Polym. Sci.* **1985**, *263*, 822.
[6] F. Jay, J.-M. Haudin, B. Monasse, *J. Mater. Sci.* **1999**, *34*, 2089.
[7] C. Duplay, B. Monasse, J.-M. Haudin, J.-L. Costa, *J. Mater. Sci.* **2000**, *35*, 6093.
[8] J. A. Kornfield, G. Kumaraswamy, A. M. Issaian, *Ind. Eng. Chem. Res.* **2002**, *41*, 6383.
[9] S. Kimata, T. Sakurai, Y. Nozue, T. Kasahara, N. Yamaguchi, T. Karino, M. Shibayama, J. A. Kornfield, *Science* **2007**, *316*, 1014.
[10] S. L. Wingstrand, B. Shen, J. A. Kornfield, K. Mortensen, D. Parisi, D. Vlassopoulos, O. Hassager, *ACS Macro Lett.* **2017**, *6*, 1268.
[11] M. R. Mackley, A. Keller, *Polymer* **1973**, *14*, 16.
[12] G. Eder, H. Janeschitz-Kriegl, S. Liedauer, in *Solidification Processes in Polymers*, Progress in Colloid and Polymer Science, Vol. 87, Springer, Berlin **1992**, p. 129.
[13] G. Eder, H. Janeschitz-Kriegl, S. Liedauer, *Prog. Polym. Sci.* **1990**, *15*, 629.
[14] B. Schrauwen, L. v. Breemen, A. Spoelstra, L. Govaert, G. Peters, H. Meijer, *Macromolecules* **2004**, *37*, 8618.
[15] J.-W. Housmans, R. J. Steenbakkers, P. C. Roozemond, G. W. Peters, H. E. Meijer, *Macromolecules* **2009**, *42*, 5728.
[16] H. Zuidema, G. W. Peters, H. E. Meijer, *Macromol. Theory Simul.* **2001**, *10*, 447.
[17] J. van Meerveld, G. W. Peters, M. Hütter, *Rheol. Acta* **2004**, *44*, 119.
[18] F. J. Custódio, R. J. Steenbakkers, P. D. Anderson, G. W. Peters, H. E. Meijer, *Macromol. Theory Simul.* **2009**, *18*, 469.
[19] N. V. Pogodina, H. H. Winter, *Macromolecules* **1998**, *31*, 8164.
[20] N. Pogodina, S. Siddiquee, J. Van Egmond, H. Winter, *Macromolecules* **1999**, *32*, 1167.
[21] N. V. Pogodina, V. P. Lavrenko, S. Srinivas, H. H. Winter, *Polymer* **2001**, *42*, 9031.
[22] G. Lamberti, G. Peters, G. Titomanlio, *Int. Polym. Process.* **2007**, *22*, 303.
[23] G. Lamberti, *Rheol. Acta* **2012**, *51*, 259.
[24] R. Pantani, V. Speranza, G. Titomanlio, *J. Rheol.* **2015**, *59*, 377.
[25] P. C. Roozemond, V. Janssens, P. van Puyvelde, G. W. Peters, *Rheol. Acta* **2012**, *51*, 97.
[26] S. Onogi, T. Asada, in *Rheology*, Springer, Boston, MA **1980**, p. 127.
[27] G. G. Fuller, "*Optical Rheometry of Complex Fluids*", Oxford University Press, New York **1995**.
[28] N. J. Wagner, *Curr. Opin. Colloid Interface Sci.* **1998**, *3*, 391.
[29] C. W. Macosko, Rheology: principles, measurements, and applications, Wiley-VCH, New York **1994**.
[30] P. T. Callaghan, *Rep. Prog. Phys.* **1999**, *62*, 599.
[31] P. T. Callaghan, A. M. Gil, *Macromolecules* **2000**, *33*, 4116.
[32] M. L. Kilfoil, P. T. Callaghan, *Macromolecules* **2000**, *33*, 6828.
[33] K. G. Hollingsworth, M. L. Johns, *J. Rheol.* **2004**, *48*, 787.
[34] P. Callaghan, in *Modern Magnetic Resonance* (Ed: G. Webb), Springer, Berlin **2006**, p. 379.
[35] M. R. Lopez-Gonzalez, W. M. Holmes, P. T. Callaghan, *Soft Matter* **2006**, *2*, 855.
[36] P. T. Callaghan, *Rheol. Acta* **2008**, *47*, 243.
[37] I. Hamley, J. Pople, C. Booth, L. Derici, M. Impéror-Clerc, P. Davidson, *Phys. Rev. E* **1998**, *58*, 7620.
[38] R. H. Somani, B. S. Hsiao, A. Nogales, S. Srinivas, A. H. Tsou, I. Sics, F. J. Balta-Calleja, T. A. Ezquerra, *Macromolecules* **2000**, *33*, 9385.
[39] V. Castelletto, I. Hamley, P. Holmqvist, C. Rekatas, C. Booth, J. Grossmann, *Colloid Polym. Sci.* **2001**, *279*, 621.
[40] V. Castelletto, I. Hamley, X.-F. Yuan, A. Kelarakis, C. Booth, *Soft Matter* **2005**, *1*, 138.
[41] E. Polushkin, S. Bondzic, J. de Wit, G. Alberda van Ekenstein, I. Dolbnya, W. Bras, O. Ikkala, G. Ten Brinke, *Macromolecules* **2005**, *38*, 1804.
[42] B. Struth, K. Hyun, E. Kats, T. Meins, M. Walther, M. Wilhelm, G. Grübel, *Langmuir* **2011**, *27*, 2880.
[43] T. Meins, K. Hyun, N. Dingenouts, M. F. Ardakani, B. Struth, M. Wilhelm, *Macromolecules* **2012**, *45*, 455.
[44] E. Stellamanns, D. Meissner, M. Lohmann, B. Struth, *J. Phys.: Conf. Ser.* **2013**, *425*, 202007.
[45] B. J. Maranzano, N. J. Wagner, *J. Chem. Phys.* **2002**, *117*, 10291.
[46] R. G. Egres, F. Nettesheim, N. J. Wagner, *J. Rheol.* **2006**, *50*, 685.
[47] M. W. Liberatore, F. Nettesheim, N. J. Wagner, L. Porcar, *Phys. Rev. E* **2006**, *73*, 020504.
[48] A. P. Eberle, L. Porcar, *Curr. Opin. Colloid Interface Sci.* **2012**, *17*, 33.
[49] M. Boulet-Audet, F. Vollrath, C. Holland, *Phys. Chem. Chem. Phys.* **2011**, *13*, 3979.
[50] M. Auriemma, A. Piscitelli, R. Pasquino, P. Cerruti, M. Malinconico, N. Grizzuti, *Eur. Polym. J.* **2015**, *63*, 123.
[51] M. A. Zadeh, A. Grande, S. van der Zwaag, S. Garcia, *RSC Adv.* **2016**, *6*, 91806.
[52] F. Zuppardi, F. R. Chiacchio, R. Sammarco, M. Malinconico, G. G. d'Ayala, P. Cerruti, *Polymer* **2017**, *112*, 169.
[53] C. Chai, N. Dixon, D. Gerrard, W. Reed, *Polymer* **1995**, *36*, 661.
[54] M.-C. Chevrel, S. Hoppe, L. Falk, B. Nadège, D. Chapron, P. Bourson, A. Durand, *Ind. Eng. Chem. Res.* **2012**, *51*, 16151.
[55] A. P. Kotula, M. W. Meyer, F. De Vito, J. Plog, A. R. Hight Walker, K. B. Migler, *Rev. Sci. Instrum.* **2016**, *87*, 105105.
[56] A. P. Kotula, K. B. Migler, *J. Rheol.* **2018**, *62*, 343.
[57] D. A. Grabowski, C. Schmidt, *Macromolecules* **1994**, *27*, 2632.
[58] M. Lukaschek, D. A. Grabowski, C. Schmidt, *Langmuir* **1995**, *11*, 3590.
[59] P. T. Callaghan, A. M. Gil, *Rheol. Acta* **1999**, *38*, 528.
[60] C. Schmidt, in *Modern Magnetic Resonance* (Ed: G. Webb), Springer, Berlin **2006**, p. 1495.
[61] K. Ohgo, F. Bagusat, T. Asakura, U. Scheler, *J. Am. Chem. Soc.* **2008**, *130*, 4182.
[62] B. Medronho, C. Schmidt, U. Olsson, M. G. Miguel, *Langmuir* **2010**, *26*, 1477.
[63] Y. Matsumiya, H. Watanabe, T. Inoue, K. Osaki, M.-L. Yao, *Macromolecules* **1998**, *31*, 7973.
[64] H. Watanabe, T. Sato, M. Hirose, K. Osaki, M.-L. Yao, *Rheol. Acta* **1998**, *37*, 519.
[65] S. Höfl, F. Kremer, H. W. Spiess, M. Wilhelm, S. Kahle, *Polymer* **2006**, *47*, 7282.
[66] S. Capaccioli, D. Prevosto, A. Best, A. Hanewald, T. Pakula, *J. Non-Cryst. Solids* **2007**, *353*, 4267.

[67] T. Meins, N. Dingenouts, J. Kübel, M. Wilhelm, *Macromolecules* **2012**, *45*, 7206.
[68] S. Kahle, W. Nussbaum, M. Hehn, H. P. Raich, M. Wilhelm, P. Blümler, *Kautsch. Gummi Kunstst.* **2008**, *61*, 92.
[69] T. Meins, K. Hyun, K.-F. Ratzsch, C. Friedrich, B. Struth, M. Wilhelm, *Ann. Trans. Nordic Rheol. Soc.* **2011**, *19*, 1.
[70] V. Räntzsch, M. Wilhelm, G. Guthausen, *Magn. Reson. Chem.* **2016**, *54*, 494.
[71] K.-F. Ratzsch, C. Friedrich, M. Wilhelm, *J. Rheol.* **2017**, *61*, 905.
[72] S. Kiewiet, V. Janssens, H. Miltner, G. van Assche, P. van Puyvelde, B. van Mele, *Rev. Sci. Instrum.* **2008**, *79*, 023905.
[73] V. Janssens, C. Block, G. van Assche, B. van Mele, P. van Puyvelde, *J. Therm. Anal. Calorim.* **2009**, *98*, 675.
[74] V. Janssens, C. Block, G. van Assche, B. van Mele, P. van Puyvelde, *Int. Polym. Process.* **2010**, *25*, 304.
[75] C. Block, B. van Mele, P. van Puyvelde, G. van Assche, *React. Funct. Polym.* **2013**, *73*, 332.
[76] I. Bruker, A. S. Lodge, *J. Rheol.* **1985**, *29*, 557.
[77] I. Bruker, *Rheol. Acta* **1986**, *25*, 501.
[78] D. N. Yemelyanov, in *Third European Rheology Conference and Golden Jubilee Meeting of the British Society of Rheology*, Springer, Dordrecht **1990**, p. 513.
[79] A. Helal, T. Divoux, G. H. McKinley, *Phys. Rev. Appl.* **2016**, *6*, 064004.
[80] V. M. Litvinov, P. A. M. Steeman, *Macromolecules* **1999**, *32*, 8476.
[81] A. Maus, C. Hertlein, K. Saalwächter, *Macromol. Chem. Phys.* **2006**, *207*, 1150.
[82] A. Papon, K. Saalwächter, K. Schäler, L. Guy, F. Lequeux, H. Montes, *Macromolecules* **2011**, *44*, 913.
[83] G. Guthausen, V. Räntzsch, C. Biquet, S. Schlabach, M. Wilhelm, *Macromol. Chem. Phys.* **2014**, *215*, 851.
[84] J. Höpfner, G. Guthausen, K. Saalwächter, M. Wilhelm *Macromolecules* **2014**, *47*, 4251.
[85] V. Räntzsch, M. Haas, M. B. Özen, K.-F. Ratzsch, K. Riazi, S. Kauffmann-Weiss, J. K. Palacios, A. J. Müller, I. Vittorias, G. Guthausen, M. Wilhelm, *Polymer* **2018**, *145*, 162.
[86] V. Räntzsch, M. B. Özen, K.-F. Ratzsch, G. Guthausen, M. Wilhelm, *AIP Conf. Proc.* **2017**, *1914*, 1.
[87] V. Räntzsch, M. B. Özen, K.-F. Ratzsch, G. Guthausen, M. Wilhelm, *AIP Conf. Proc.* **2017**, *1843*, 1.
[88] K. Hongladarom, V. Ugaz, D. Cinader, W. Burghardt, J. Quintana, B. Hsiao, M. Dadmun, W. Hamilton, P. Butler, *Macromolecules* **1996**, *29*, 5346.
[89] J. Berghausen, J. Zipfel, O. Diat, T. Narayanan, W. Richtering, *Phys. Chem. Chem. Phys.* **2000**, *2*, 3623.
[90] A. Nogales, B. S. Hsiao, R. H. Somani, S. Srinivas, A. H. Tsou, F. J. Balta-Calleja, T. A. Ezquerra, *Polymer* **2001**, *42*, 5247.
[91] R. H. Somani, B. S. Hsiao, A. Nogales, H. Fruitwala, S. Srinivas, A. H. Tsou, *Macromolecules* **2001**, *34*, 5902.
[92] R. H. Somani, L. Yang, B. S. Hsiao, P. K. Agarwal, H. A. Fruitwala, A. H. Tsou, *Macromolecules* **2002**, *35*, 9096.
[93] P. K. Agarwal, R. H. Somani, W. Weng, A. Mehta, L. Yang, S. Ran, L. Liu, B. S. Hsiao, *Macromolecules* **2003**, *36*, 5226.
[94] G. Kumaraswamy, R. K. Verma, J. A. Kornfield, F. Yeh, B. S. Hsiao, *Macromolecules* **2004**, *37*, 9005.
[95] L. Balzano, N. Kukalyekar, S. Rastogi, G. W. Peters, J. C. Chadwick, *Phys. Rev. Lett.* **2008**, *100*, 048302.
[96] L. Balzano, S. Rastogi, G. W. Peters, *Macromolecules* **2009**, *42*, 2088.
[97] G. Portale, D. Cavallo, G. C. Alfonso, D. Hermida-Merino, M. v. Drongelen, L. Balzano, G. Peters, J. Goossens, W. Bras, *J. Appl. Crystallogr.* **2013**, *46*, 1681.
[98] Z. Ma, L. Balzano, G. W. Peters, *Macromolecules* **2012**, *45*, 4216.
[99] Z. Ma, L. Balzano, G. Portale, G. W. Peters, *Polymer* **2014**, *55*, 6140.
[100] L. Balzano, Z. Ma, D. Cavallo, T. B. van Erp, L. Fernandez-Ballester, G. W. Peters, *Macromolecules* **2016**, *49*, 3799.
[101] M. van Drongelen, D. Cavallo, L. Balzano, G. Portale, I. Vittorias, W. Bras, G. C. Alfonso, G. W. Peters, *Macromol. Mater. Eng.* **2014**, *299*, 1494.
[102] J. M. Samon, J. M. Schultz, J. Wu, B. Hsiao, F. Yeh, R. Kolb, *J. Polym. Sci., Part B: Polym. Phys.* **1999**, *37*, 1277.
[103] J. Schultz, B. S. Hsiao, J. Samon, *Polymer* **2000**, *41*, 8887.
[104] R. Kolb, S. Seifert, N. Stribeck, H. Zachmann, *Polymer* **2000**, *41*, 1497.
[105] P. Panine, M. Gradzielski, T. Narayanan, *Rev. Sci. Instrum.* **2003**, *74*, 2451.
[106] E. Polushkin, G. A. van Ekenstein, O. Ikkala, G. t. Brinke, *Rheol. Acta* **2004**, *43*, 364.
[107] P. Pfleiderer, S. J. Baik, Z. Zhang, G. Vleminckx, M. P. Lettinga, E. Grelet, J. Vermant, C. Clasen, *Rev. Sci. Instrum.* **2014**, *85*, 065108.
[108] B. Pulamagatta, E. Ostas, F. Herbst, B. Struth, W. H. Binder, *Eur. Polym. J.* **2012**, *48*, 1127.
[109] M. Lettinga, P. Holmqvist, P. Ballesta, S. Rogers, D. Kleshchanok, B. Struth, *Phys. Rev. Lett.* **2012**, *109*, 246001.
[110] S. Kim, K. Hyun, Y. S. Kim, B. Struth, C. Clasen, K. H. Ahn, *Langmuir* **2013**, *29*, 10059.
[111] F. Westermeier, D. Pennicard, H. Hirsemann, U. H. Wagner, C. Rau, H. Graafsma, P. Schall, M. P. Lettinga, B. Struth, *Soft Matter* **2016**, *12*, 171.
[112] T. Yan, B. Zhao, Y. Cong, Y. Fang, S. Cheng, L. Li, G. Pan, Z. Wang, X. Li, F. Bian, *Macromolecules* **2010**, *43*, 602.
[113] Y. Liu, W. Zhou, K. Cui, N. Tian, X. Wang, L. Liu, L. Li, Y. Zhou, *Rev. Sci. Instrum.* **2011**, *82*, 045104.
[114] J. Champion, L. Gate, G. Meeten, P. Wood, *Colloids Surf. A* **1996**, *111*, 223.
[115] S. Paulin, B. J. Ackerson, M. Wolfe, *Phys. Rev. E* **1997**, *55*, 5812.
[116] A. Montesi, A. A. Peña, M. Pasquali, *Phys. Rev. Lett.* **2004**, *92*, 058303.
[117] M. Kawaguchi, K. Kubota, *Langmuir* **2004**, *20*, 1126.
[118] J. Berghausen, J. Fuchs, W. Richtering, *Macromolecules* **1997**, *30*, 7574.
[119] L. M. Walker, W. A. Kernick, N. J. Wagner, *Macromolecules* **1997**, *30*, 508.
[120] J. Bossart, H. C. Oettinger, *Macromolecules* **1995**, *28*, 5852.
[121] M. C. Friedenberg, G. G. Fuller, C. W. Frank, C. R. Robertson, *Macromolecules* **1996**, *29*, 705.
[122] T. Kume, T. Hashimoto, T. Takahashi, G. G. Fuller, *Macromolecules* **1997**, *30*, 7232.
[123] J. A. Pathak, S. D. Hudson, *Macromolecules* **2006**, *39*, 8782.
[124] Z.-R. Chen, J. A. Kornfield, *Polymer* **1998**, *39*, 4679.
[125] R. M. Kannan, J. A. Kornfield, *Macromolecules* **1994**, *27*, 1177.
[126] W. Dietz, J. L. White, E. S. Clark, *Polym. Eng. Sci.* **1978**, *18*, 273.
[127] K. Lee, M. Mackley, *Chem. Eng. Sci.* **2001**, *56*, 5653.
[128] A. Elmoumni, H. H. Winter, A. J. Waddon, H. Fruitwala, *Macromolecules* **2003**, *36*, 6453.
[129] M. R. Mackley, *Colloid Polym. Sci.* **1975**, *253*, 373.
[130] D. G. Hassell, M. R. Mackley, *Rheol. Acta* **2008**, *47*, 435.
[131] M. R. Mackley, G. D. Moggridge, O. Saquet, *J. Mater. Sci.* **2000**, *35*, 5247.
[132] L. Scelsi, M. R. Mackley, *Rheol. Acta* **2008**, *47*, 895.
[133] M. R. Mackley, F. C. Frank, A. Keller, *J. Mater. Sci.* **1975**, *10*, 1501.
[134] A. Elmoumni, R. A. Gonzalez-Ruiz, E. B. Coughlin, H. H. Winter, *Macromol. Chem. Phys.* **2005**, *206*, 125.
[135] A. Elmoumni, H. H. Winter, *Rheol. Acta* **2006**, *45*, 793.
[136] R. Pantani, I. Coccorullo, V. Volpe, G. Titomanlio, *Macromolecules* **2010**, *43*, 9030.
[137] R. Pantani, V. Nappo, F. De Santis, G. Titomanlio, *Macromol. Mater. Eng.* **2014**, *299*, 1465.

[138] F. De Santis, R. Pantani, G. Titomanlio, *Polymer* **2016**, *90*, 102.
[139] E. Koscher, R. Fulchiron, *Polymer* **2002**, *43*, 6931.
[140] J.-W. Housmans, G. W. Peters, H. E. Meijer, *J. Therm. Anal. Calorim.* **2009**, *98*, 693.
[141] J. E. Mark, "*Physical Properties of Polymers Handbook*", Springer, New York **2007**.
[142] M. Avrami, *J. Chem. Phys.* **1941**, *9*, 177.
[143] J. Mewis, N. J. Wagner, "*Colloidal Suspension Rheology*", Cambridge University Press, New York **2012**.
[144] S. Mueller, E. Llewellin, H. Mader, *Proc. R. Soc. London, Ser. A* **2010**, *466*, 1201.
[145] P. H. Hermans, "*Contribution to the Physics of Cellulose Fibres*", Elsevier, Amsterdam **1946**.
[146] J. L. White, J. E. Spruiell, *Polym. Eng. Sci.* **1983**, *23*, 247.